Materials and Design 122 (2017) 220–225

Contents lists available at ScienceDirect

Materials and Design

journal homepage: www.elsevier.com/locate/matdes

Tunable bandgap and spin-orbit coupling by composition control of MoS_2 and MoO_x (x = 2 and 3) thin film compounds

S. Erfanifam[a,*], S.M. Mohseni[a,*], L. Jamilpanah[a], M. Mohammadbeigi[a], P. Sangpour[b], S.A. Hosseini[c], A. Iraji Zad[c,d]

[a]Department of Physics, Shahid Beheshti University, Tehran, G. C., Evin, Tehran 19839, Iran
[b]Department of Nanotechnology and Advanced Materials, Materials and Energy Research Center, Karaj, Iran
[c]Institute for Nanoscience and Nanotechnology (INST), Sharif University of Technology, Tehran, Iran
[d]Faculty of Physics, Sharif University of Technology, P.O.Box 11155-9161,Tehran, Iran

HIGHLIGHTS

- A composite form of MoS_2, MoO_2 and MoO_3 thin film was electrodeposited.
- The relative content of these compounds was changed in different thickness of the layers.
- The bandgap and type of semiconductivity were tuned by change on the composition.
- Spin-orbit coupling of Mo 3d doublet was enhanced by composition control.

GRAPHICAL ABSTRACT

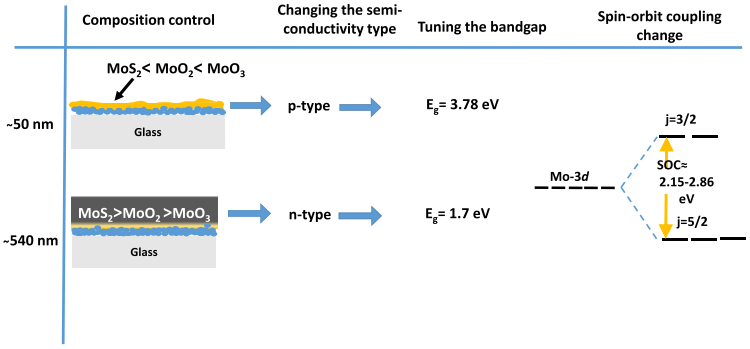

ARTICLE INFO

Article history:
Received 2 November 2016
Received in revised form 17 February 2017
Accepted 27 February 2017
Available online 2 March 2017

JEL classification:
2010 MSC 00-01
99-00

Keywords:
Low dimensional dichalcogenide compounds
X-ray photoelectron spectroscopy
Optical and electrical bandgaps

ABSTRACT

We report on the MoS_2 and MoO_x (x = 2 and 3) composite thin layers, electrodeposited, onto a Florine doped Tin Oxide (FTO) substrate. Our results show a change in relative content of these compounds in different thicknesses ranging from ~20 to 540 nm. This change in the relative content at different thicknesses leads to a change in optical and electrical properties including bandgap and the type of semiconductivity. A sharp transition from p to n-type of semiconductivity is observed by scanning tunneling spectroscopy measurements. We find that the spin-orbit interaction of Mo 3d electrons in the MoS_2 and MoO_3 enhances by significant reduction of the MoO_3 content in thicker layers.

1. Introduction

In the past decade, low dimensional binary compounds with general formula MX_2, have attracted significant attention due to some unique properties of them [1–4]. In these compounds M is usually a transition metal and X is a chalcogenide. Among them probably Molybdenum disulfide (MoS_2) is the most well-known material. MX_2 compounds have potential applications in nanoelectronics, photoelectrochemistry, energy storage , etc. [5–12]. However, in a form of single MX_2 compound, bandgap can be tuned by back-gate control or by impurity doping, but it technically requires some

* Corresponding authors.
E-mail addresses: s.erfanifam@gmail.com (S. Erfanifam), m-mohseni@sbu.ac.ir.

http://dx.doi.org/10.1016/j.matdes.2017.02.085
0264-1275/

additional preparation steps [13,14]. Hybrid configuration of the MX_2 compounds can overcome this drawback. By appropriate combination of these binary compounds, different bandgaps can be obtained.

Various techniques such as chemical vapor deposition [15,17] or mechanical (liquid phase) exfoliation have been employed for fabrication of transition metal dichalcogenide compounds, but there are few attempts by electrodeposition [16,18-20]. This technique can provide low cost and high quality structures with controllable size made of various compounds. During the fabrication process of the MoS_2 from Mo oxide compounds there are naturally MoO_x products; results in MoS_2 and MoO_x composition.

In order to exploit electrical and optical properties of the MoS_2 and MoO_x (x=2 and 3) composition at first, some of their important properties should be referred, independently. In the monolayer MoS_2, the inversion symmetry is broken that results in a relatively (compared to the other transition metals) strong spin-orbit coupling in the Mo 3d electrons. This coupling leads to the valence band splitting which is abbreviated as SOS. The SOS in bilayer MoS_2 mostly comes from inter-layer coupling. The strong SOS can lead to some important excitonic effects which are detectable using various techniques. The SOS value reported for this compound is around 150 meV.

MoO_2 is an unusual metal oxide which exhibits metal-like electrical conductivity (semimetal or a wide bandgap n-type semiconductor in bulk) [21,22]. During the last decade, optical and structural properties of this compound have been thoroughly investigated. MoO_2 is a mixed ionic electronic conductor [23] and its electrical resistivity is very controversial. The SOS value of this material is less than that of MoS_2 at which is around 130 meV.

Molybdenum trioxide (MoO_3), with an orthorhombic symmetry is intrinsically n-type semiconductor with 3.2 eV bandgap. It has been widely investigated due to its high work function [24] and intercalation of Li^+ and H^+ ions [25]. These properties make it a promising candidate for photorechargeable and photoelectrochemical applications[26–28]. In contrast to the MoS_2 and the MoO_2, this compound does not exhibit any symmetry-breaking valence band splitting.

The present paper explores the structural and optical properties of the electrodeposited MoS_2, MoO_2 and MoO_3 compounds made on transparent FTO substrate. However, according to Ref. [16] a transition metal substrate is required to act as catalyst to have MoS_2, but this research proves that it is possible to have a composition of these compounds on a transparent substrate of the FTO. This paper provides a fabrication recipe to control each of these (MoS_2, MoO_2, MoO_3) compounds and report on their interesting properties. In particular, this paper discusses on the optical (electrical) bandgap, spin-orbit coupling (SOC) and SOS of the Mo 3d electrons by change on the composition in different thickness of the layers.

2. Experiment

DC electrodeposition was carried out at room temperature to make thin layers from an electrolyte containing sodium molybdate ($Na_2Mo_2O_4$) (0.5 M) with disodium sulfide ($Na_2S.5H_2O$) (30 g /l) similar to Ref. [16]. The pH value of the electrolyte was adjusted to 7 by adding dilute sulfuric acid. The products of chemical reactions in this solution depending on the electrodeposition conditions (substrate, temperature, pH and applied potential), can be MoS_2 and MoO_x(x=2 and 3).

A two electrode potentiostat having Pt as anode and FTO substrate as cathode was employed for the electrodeposition in this single-bath solution. Before electrodeposition, the FTO substrate was cleaned by ethanol and distilled water. Then the sample was located in a home-made chemical cell in front of a Pt counter electrode. A magnetic stirrer was used to mix the solution during deposition. In a series of samples the electrodeposition was performed at different deposition times between 7 s and 10 min (7 s, 15 s, 30 s, 1 min, 2 min, 10 min) to achieve various thickness of the layers. Profilometry of the fabricated samples displayed the thickness from ~ 20 to 540 nm (±5nm). Applied DC potential was adjusted to 2.5 V (the minimum required potential for deposition from this electrolyte on the FTO) for all samples in which the current density during the deposition was kept at around 2 mA/cm^2, well below 10 mA/cm^2 in accordance with previous reports to avoid reduction of MoO^{2+} ions as much as possible. The thick layers were black while thinner ones, below 1 min deposition time, were amber yellow and more transparent. The composition of the layers was expected to be affected by the interplay between H^+ and Oxygen. This interplay in chemical reactions resulted in the change on final products and composition.

3. Results and discussion

3.1. Structural characteristics

In this paper, mainly the results obtained from the thinnest and thickest layers are discussed which exhibit significant changes in optical and electrical properties. Fig. 1, illustrates the morphology and composition of the electrodeposited thin layers in two different thicknesses. Fig. 2a and b shows SEM micrograph of as-deposited samples with different deposition times of 30 s (with 100 nm thickness) and 10 min (with 540 nm thickness) respectively. It is clearly seen that at thinner one roughness of the substrate affects on the morphology of the layer, While thicker one shows large-scale flat islands. Fig. 2c and d exhibits TEM and selected area diffraction pattern (SAED) of the thicker composite layer. Interestingly, it is clearly seen that the structure of the fabricated composite is mostly polycrystalline. A rough orientation of the crystals, attributed to the MoO_2 and MoS_2 structures, is calculated from spot patterns.

In order to understand the chemical composition and for accurate analysis, XPS (X-ray photoelectron spectroscopy) spectra of the 30 s and 10 min as-deposited samples (shown in Fig. 3) were acquired. The obtained XPS data from 0 to 1200 eV is convoluted to analyze the XPS peaks. Best fitted Gaussian curves is used to determine the peak positions presented in Table 1. C 1 s calibration peak (284.8 eV) is employed to find the correct binding energy of all peaks.

According to Table 1, the relative content of the MoS_2 has noticeable increase from 20 % to 43 %. This enhancement comes from less Oxygen evolution as well as less substrate effects on the thicker layer. However, chemical stability of MoO_3 is the highest among these three compounds, the content of that decreases at higher deposition times and higher thicknesses.

The Molybdenum and Sulfur binding energies of each compound for two different thicknesses of the composite layer are shown in Table 2. Peak position of Oxygen is not shown due to the substrate effect and not possible accurate conclusion. In the XPS experiment, usually charge density around emitted-photoelectron has inverse relation with the binding energy, due to the repulsive Coulombic force of the electrons around a photoelectron. It is observed that, in the 100 nm sample, the peaks are shifted towards higher energies because of more formation of the MoO_2 and the MoO_3 compounds, indicating low density of the electrons. In contrast,energy downshift of the spectral peaks by increasing of the MoS_2 content in 540 nm sample can indicate higher density of the electrons.

Fig. 4 shows the SOC of the Mo 3d electrons in the MoS_2 at different thickness of the layer. The SOC, calculated from Mo $3d_{3/2}$ and Mo $3d_{5/2}$ peaks, increases from 2.15 to 2.86 eV at thicker layer. This effect is connected to the relative increasing of the MoS_2 content. The observed SOC data are in agreement with reported results by several researches (as an example, see Senthilkumar et al. [29]). According to Table 2, the SOC of Mo 3d electrons in the MoO_3 steps up from 3.28 to 3.74 eV. As it is expected the SOC in the MoO_3 is higher than the

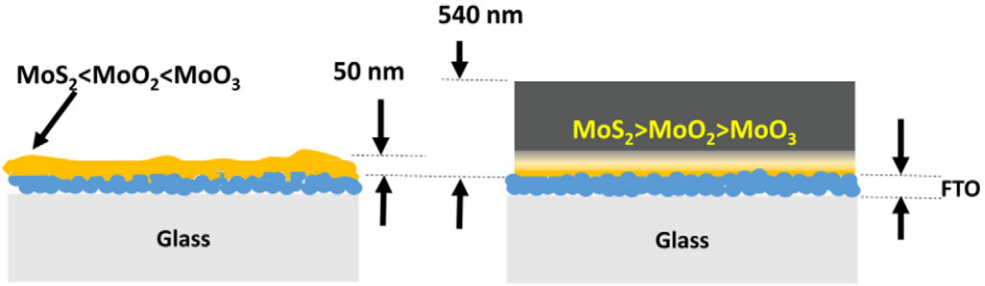

Fig. 1. Schematic representation of two distinct samples with 50 and 540nm thickness. Morphology and relative content change are shown qualitatively by color gradient at thinner and thicker samples relatively.

MoO_2 because of direct relation between molecular mass and SOC. In addition, 2p peaks of the sulfur in the MoS_2 increases from 1.4 to 1.55 eV.

In the monolayer or bulk MoX_2 (x=O and S) compounds, inversion symmetry breaking or interlayer coupling, can lead to the valence and conduction band splittings in first Brillouin zone. The excitonic peaks that have arisen from this splitting are usually shown in the UV-Vis experiments. Apparently, in this composition, the valence band splitting is absent. With this, one can conclude that the presence of MoO_2 and MoO_3 suppress the valence band splitting. The Key point is that this splitting mostly depends on the SOS and crystal symmetries rather than SOC. The correlation between SOC and SOS for this composition is not very clear yet.

3.2. Optical and electrical properties

In the optoelectronics and material science, optical absorption measurements by UV-Vis spectroscopy is a powerful and common characterization technique. Fig. 5a shows the UV-Vis spectrum for different deposition times. Interestingly, by probing from 300 to 1100 nm various anomalies and peaks, attributed to the intraband and interband transitions, are observed by a redshift for thinner layers. The low energy peaks (where the excitonic peaks was expected to be observed), does not exactly coincide to the reported values of 623 and 683 nm for MoS_2 and neither very well separated from each other. However, high energy peaks related to interband transitions are in agreement with reported results.

Coexistence of the MoO_2 and the MoS_2 in this composition, can explain the absence of the excitonic peaks in UV-Vis spectrum at around 623 nm and 683 nm. It seems screening of the valence band splitting in the MoS_2 by the valence band splitting in the MoO_2 has significant effect on the possible suppression of the excitonic peaks in the UV-Vis spectrum. Illustration of this behavior is schematically presented in inset of the 5.a. This behavior causes energy separation of the Mo 3d degeneracy-lifted orbitals (due to the SOS coming from inversion symmetry breaking or inter-layer coupling) to be in both compounds beyond the resolution of the UV-Vis instrument. However, in this composition, the MoO_3 is also present, but no contribution due to excitonic effects is expected. Overall, these UV-Vis results had characteristics of the both MoS_2 and MoO_x compounds

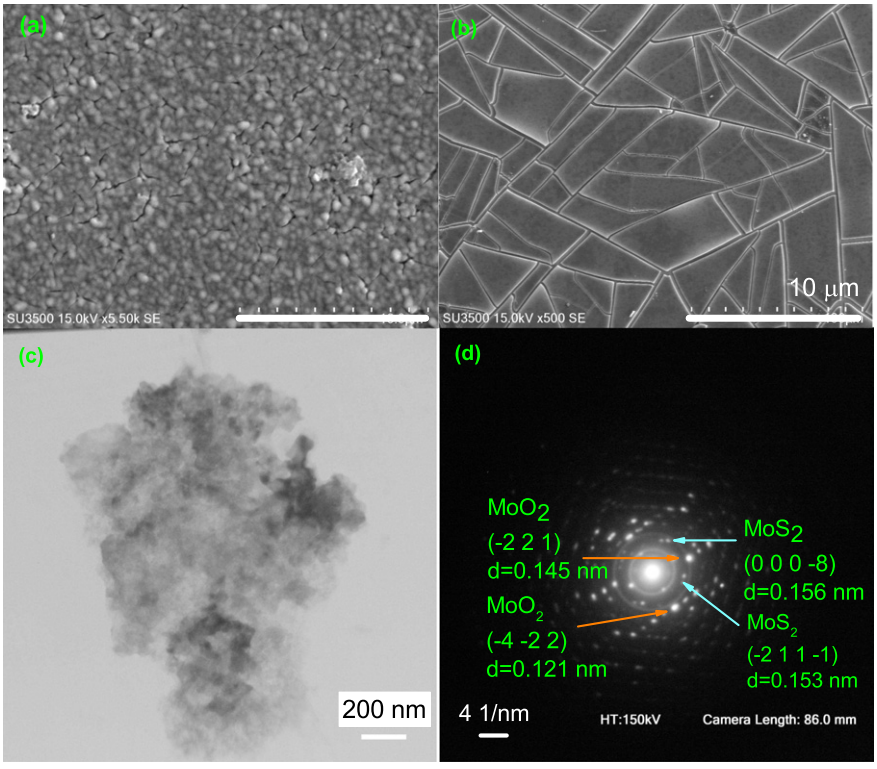

Fig. 2. SEM micrograph of the:(a) thin and;(b) thick layers exhibiting morphology and substrate effects;(c) TEM and;(d) SAED pattern of the thicker layer. From SAED pattern at least two series of points can be attributed to the MoS_2 and MoO_2 compounds.

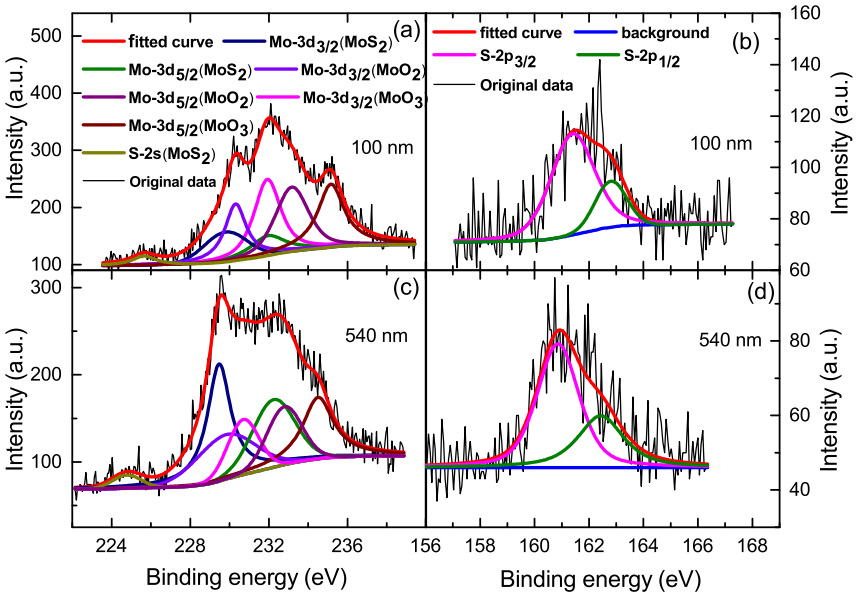

Fig. 3. XPS spectra of the Mo 3d and S 2p electrons coincide to the binding energies of the Mo in the MoS_2, MoO_2 and MoO_3 compounds at; (a, b) 100 nm and; (c, d) 540 nm layers.

Table 1
Relative content of compounds in as-deposited samples.

Compound	MoS_2	MoO_2	MoO_3
Relative content (100 nm)	0.20	0.36	0.43
Relative content (540 nm)	0.43	0.29	0.28

Refs.[30,31]. It is worth to note that (by comparison of the insets in Figs. 5 and 4), the SOS and the SOC have two different origins. As it was discussed above, the first one is due to the inversion symmetry breaking or inter-layer coupling and the second one comes from the spin-orbit coupling of Mo 3d electrons ($J = L \pm S$, $L = 2$ and $S = 1/2$).

Usually, the optical bandgap of the semiconductors can be calculated by plotting $(\alpha h\nu)^2$ versus $h\nu$ in UV-Vis spectrum where α is absorption coefficient (Tauc plot). Fig. 5b shows the Tauc plot of indirect bandgap obtained from different thicknesses. The calculations indicate 3.78 eV energy gap for thinnest layer with 7 s deposition time, while the bandgap for 10 min deposited one is 1.77 eV. Complementary experiments for the deposition times, between these two values, exhibits a systematic and tunable bandgap. From this, it can be concluded that the bandgap is not strongly affected by dislocations or impurities.

Interestingly, an unusual step-like behavior below 15 s deposition time is observed. Such behavior can be attributed to the curved shape of layer which is formed on top of the rough FTO substrate. The FTO is made of the Florine doped Tin oxide nanoparticles (with approximately 200 nm particle diameter) deposited on a glass. This bending of the electrodeposited layer caused a lattice distortion and affect the band structure. Our extended experiments at 5 V and 7.5 V (not shown here) showed no significant change on these features. The electrical bandgaps obtained from scanning tunneling spectroscopy measurements (NAMA-STM SS3) provided additional information about carrier correlations and charge densities. Fig. 6 exhibits the scanning tunneling spectroscopy of two samples with different thicknesses. Interestingly, it was observed that by increasing the thickness, bandgap decreases from 3.3 to 3 eV. According to these measurements the optical and electrical bandgaps are comparable. In addition, Fermi energy distance from conduction band decreases (from 2 to 1.2 eV), indicating a change from p-to n-type of the semiconductivity. At first approximation, the origin of this behavior can be ascribed to the composition change. A detailed explanation, based on the layer growth mechanism and the related parameters is offered as following. In the beginning of deposition, due to catalytic effect of the substrate, the protons penetrates and forms a bound state with Oxygen atoms to form water molecules that leaves Oxygen vacancies behind. This vacancies make the semiconductor p-type. After a while and separation of layer-growing points from FTO substrate, catalytic effect of the substrate is going to be smeared out. Accordingly, the Oxygen evolution decrease concomitant with the higher sulfur evolution leading to a higher electron charge density.

4. Conclusions

In conclusion, the MoS_2 and the MoO_x($x = 2$ and 3) composites were electrodeposited on a transparent (FTO) substrate in the form of thin films with different thicknesses. The Optical and electrical

Table 2
Binding energy of Mo and S in as-deposited samples. Summary of the peak positions, spin-orbit coupling and related shifts in the Mo 3d and S 2p for 100nm and 540nm films.

	Mo $3d_{3/2}$	Mo $3d_{5/2}$	Δ_{SOC}(Mo 3d)	S-$2p_{1/2}$	S-$2p_{3/2}$	Δ_{SOC}(S 2p)
100 nm						
MoS_2	231.97	229.98	2.15	161.40	162.80	1.38
MoO_2	233.18	230.30	2.85			
MoO_3	235.15	231.96	3.28			
540 nm						
MoS_2	232.24	229.47	2.87	160.86	162.43	1.53
MoO_2	232.79	229.81	2.77			
MoO_3	234.50	230.69	3.74			

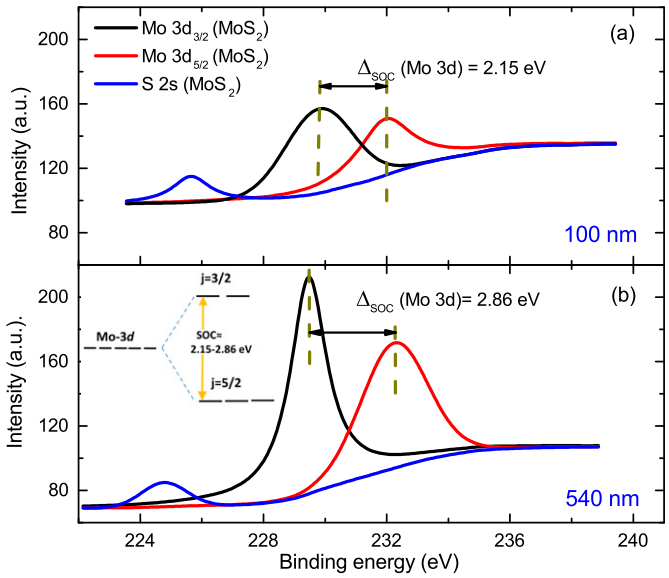

Fig. 4. Spin-orbit coupling of the Mo 3d electrons in MoS_2 for two different thickness. 2s peaks of the sulfur exhibit a significant downshift towards low binding energy. Inset in (b) shows schematic representation of the spin-orbit coupling of L = 2 and S = 1/2 in 3d orbitals.

characteristics were tuned by composition. This tunability enabled us to control the bandgap and the type of semiconductivity. The XPS and UV-Vis results demonstrated that the MoO_2 can suppress the SOS and valence band splitting of the MoS_2 compound. In addition, the SOC of the Mo 3d electrons were enhanced in the composites with higher MoS_2 content. This research suggests investigation of the electrodeposited hybrid chalcogenide compounds based on the composition control.

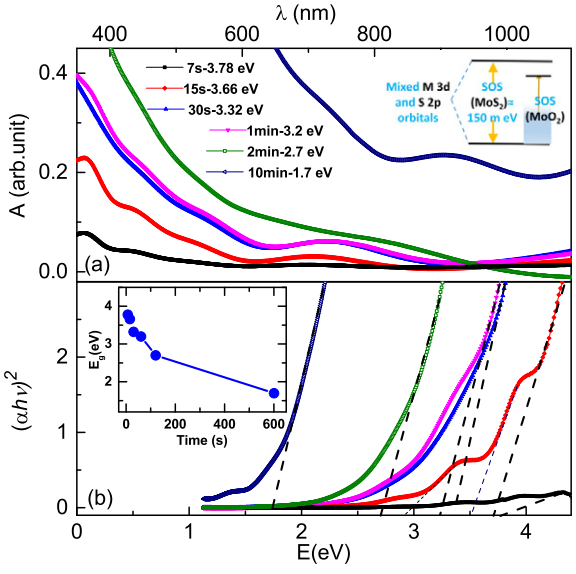

Fig. 5. (a) UV-Vis spectrum of the as-deposited thin films with different deposition times; (b) Tauc plot and bandgap (inset). The broad absorption band centered at 416 nm (2.98 eV) arising from the complicated interaband transitions is also observed. However the excitonic peaks of spin orbit and interlayer couplings are not well resolved. The inset shows screening effect of MoO_2 valence band splitting on MoS_2 schematically.

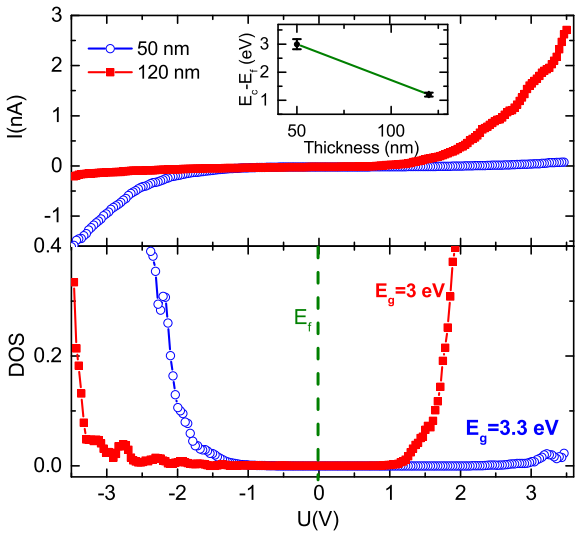

Fig. 6. Scanning tunneling spectroscopy and DOS of the thick and thin films. Inset shows E_c-E_f change versus layer thickness.

Acknowledgments

Salim Erfanifam acknowledges the support from the Iranian Elites foundation. S. M. Mohseni acknowledges ISEF foundation.

Appendix A. Supplementary data

Supplementary data to this article can be found online at http://dx.doi.org/10.1016/j.matdes.2017.02.085.

References

[1] L.F. Mattheis, Energy bands for 2H-$NbSe_2$ and 2H-MoS_2, Phys. Rev. Lett. 30 (1973) 784.
[2] K.F. Mak, C. Lee, J. Hone, J. Shan, T.F. Heinz, Atomically thin MoS_2 a new direct-gap semiconductor, Phys. Rev. Lett. 105 (2010) 136805.
[3] R. Coehoorn, C. Haas, J. Dijkstra, C.J.F. Flipse, R.A de Groot, A. Wold, Electronic structure of $MoSe_2$, MoS_2, and WSe_2. I. Band-structure calculations and photoelectron spectroscopy, Phys. Rev. B 35 (1987) 6195.
[4] X. Yin, Z. Ye, D.A. Chenet, Y. Ye, K.O. Brien, J.C. Hone, X. Zhang, Edge nonlinear optics on a MoS_2 atomic monolayer, Science 344 (2014) 488–490.
[5] Y.L. Huang, Y. Chen, W. Zhang, S.Y. Quek, Chen. Chang-Hsiao, Li. Lain-Jong, Wei-Ting. Hsu, Wen-Hao. Chang, Y.J. Zheng, W. Chen, A.n.d.r.e.w.T.S. Wee, Bandgap tuneability at single-layer molybdenum disulphide grain boundaries, Nat. Commun. 6 (2015) 6298.
[6] J. Klinovaja, D. Loss, Spintronics in MoS_2 monolayer quantum wires, Phys. Rev. B. 88 (2013) 075404.
[7] A. Bandyopadhyay, S.K. Pati, Tuning the opto-electronic properties of MoS_2 layer using charge transfer interactions: effect of different donor molecules, Mater. Res. Express 2 (2015) 085003.
[8] J. He, L. Chen, Z.O. Yi, Chak-Tong. Au, Shuang-Feng. Yin, CdS nanorods coupled with WS_2 nanosheets for enhanced photocatalytic hydrogen evolution activity, Ind. Eng. Chem. Res. 55 (30) (2016) 8327–8333.
[9] X. Zhang, Q. Zhang, Y. Sun, P. Zhang, X. Gao, W. Zhang, J. Guo, MoS_2-graphene hybrid nanosheets constructed D architectures with improved electrochemical performance for lithium-ion batteries and hydrogen evolution, Electrochim. Acta 189 (2016) 224–230.
[10] Z. Yufei, Z. Yuxia, Y. Zhiyu, Y. Yiming, S. Kening, Synthesis of MoS_2 and MoO_2 for their applications in H_2 generation and lithium ion batteries: a review, Sci. Technol. Adv. Mater. 14 (2013) 043501.
[11] J.A. Wilson, A.D. Yoffe, The transition metal dichalcogenides discussion and interpretation of the observed optical, electrical and structural properties, Adv. Phys. 18 (1969) 193.
[12] R.S. Patil, M.D. Uplane, P.S. Patil, Electrosynthesis of electrochromic molybdenum oxide thin films with rod-like features, Int. J. Electrochem. Sci. 3 (2008) 259–265.
[13] L. Chih-Pin, L. Guohong, M. Jinhai, W. Li-Min, Y.A. Eva, Bandgap, mid-gap states, and gating effects in MoS_2, Nano Lett 14 (8) (2014) 4628–4633.
[14] J. Lee, K.F. Mak, J. Shan, Electrical control of the valley Hall effect in bilayer MoS_2 transistors, Nature Nanotech. 11 (2016) 421–425.

[15] Y. Zhan, Z. Liu, S. Najmaei, P.M. Ajayan, J. Lou, Large-area vapor-phase growth and characterization of MoS_2 atomic layers on a SiO_2 substrate., 14(8). 2012, 966–971.
[16] S.K. Ghosh, C. Srivastava, S. Nath, J.P. Celis, Simple formation of nanostructured molybdenum disulfide thin films by electrodeposition, Int. J. Electrochem. 7 (2013) 2013.
[17] H. Bergeron, V.K. Sangwan, J.J. McMorrow, G.P. Campbell, I. Balla, X. Liu, M.J. Bedzyk, T.J. Marks, Mark C. Hersam, Chemical vapor deposition of monolayer MoS_2 directly on ultrathin Al_2O_3 for low-power electronics, Appl. Phys. Lett. 110 (2017) 053101.
[18] E.A. Ponomarev, M.N. Spallart, G. Hodes, C.L. Clement, Electrochemical deposition of MoS_2 thin films by reduction of tetrathiomolybdate, Thin Solid Films 280 (1996) 86.
[19] S. Murugesan, A. Akkineni, B.P. Chou, M.S. Glaz, D.A.V. Bout, K.J. Stevenson, Room temperature electrodeposition of molybdenum sulfide for catalytic and photoluminescence applications, Acs Nano 7 (2013) 8199–8205.
[20] B.D. Falola, T. Wiltowski, I.I. Suni, Electrodeposition of MoS_2 for charge storage in electrochemical supercapacitors, J. Electrochem. Soc. 163 (9) (2016) 568–574.
[21] J. Moosburger-Will, J. Kündel, M. Klemm, S. Horn, P. Hofmann, U. Schwingenschlögl, V. Eyert, Fermi surface of MoO2 studied by angle-resolved photoemission spectroscopy, de Haas-van Alphen measurements, and electronic structure calculations, Phys. Rev. B. 79 (1997) 115113.
[22] V. Eyert, R. Horny, K.H. Höck, S. Horn, Embedded Peierls instability and the electronic structure of MoO_2, J. Phys. Condens. Matter 12 (2000) 4923–4946.
[23] K.W. Harrison, C.D. Corolewski, M.D. McCluskey, J. Lindemuth, S. Ha, M.G. Norton, Electronic transport in molybdenum dioxide thin films, J. Mater. Sci.: Mater. Electron. 26 (2015) 9717–9720.
[24] Y. Guo, J. Robertson, Origin of the high work function and high conductivity of MoO_3, Appl. Phys. Lett. 105 (2014) 222110.
[25] S. Balendhran, S. Walia, H. Nili, J.Z. Ou, S. Zhuiykov, R.B. Kaner, S. Sriram, M. Bhaskaran, K. Kalantar-zadeh, Two-dimensional molybdenum trioxide and dichalcogenides, Adv. Funct. Mater 23 (2013) 3952–3970.
[26] S.N. Lou, N. Yap, J. Scott, R. Amal, Y.H. Ng, Influence of MoO_3 (110) crystalline plane on its self-charging photoelectrochemical properties, Sci. Rep. 4 (2014) 7428.
[27] S.N. Lou, Y.H. Ng, C. Ng, J. Scott, R. Amal, Harvesting, storing and utilising solar energy using MoO_3: modulating structural distortion through pH adjustment, ChemSusChem 7 (7) (2014) 1934–1941.
[28] D.D. Yao, J.Z. Ou, K. Latham, S. Zhuiykov, A.P.O. Mullane, K. Kalantar-zadeh, Electrochromic properties of TiO_2 nanotubes coated with electrodeposited MoO_3, Cryst, Growth Des. 7 (7) (2012) 1865–1870.
[29] V. Senthilkumar, L.C. Tam, Y.S. Kim, Y. Sim, M.J. Seong, J.I. Jang, Direct vapor phase growth process and robust photo-luminescence properties of large area MoS_2 layers, Nano Res. 17 (2014) 1175–1184.
[30] B. Visic, R. Dominko, M.K. Gunde, N. Hauptman, S.D. Skapin, M. Remskar, Optical properties of exfoliated MoS_2 coaxial nanotubes-analogues of graphene, Nanoscale Res. Lett. 6 (2011) 593.
[31] M.B. Sreedhara, H.S.S. Ramakrishna Matte, A. Govindaraj, C.N.R. Rao, Synthesis, characterization, and properties of few-layer MoO_3, Chem Asian J. 8 (2013) 2430–2435.